

# Texture-aware and Shape-guided Transformer for Sequential DeepFake Detection

Yunfei Li<sup>1</sup> Yuezun Li<sup>1,\*</sup> Xin Wang<sup>2</sup> Jiaran Zhou<sup>1</sup> Junyu Dong<sup>1</sup>

<sup>1</sup> College of Computer Science and Technology,  
Ocean University of China, Qingdao, China

<sup>2</sup> University at Albany, SUNY,

## Abstract

Sequential DeepFake detection is an emerging task that aims to predict the manipulation sequence in order. Existing methods typically formulate it as an image-to-sequence problem, employing conventional Transformer architectures for detection. However, these methods lack dedicated design and consequently result in limited performance. In this paper, we propose a novel Texture-aware and Shape-guided Transformer to enhance detection performance. Our method features four major improvements. Firstly, we describe a texture-aware branch that effectively captures subtle manipulation traces with the Diversiform Pixel Difference Attention module. Then we introduce a Bidirectional Interaction Cross-attention module that seeks deep correlations among spatial and sequential features, enabling effective modeling of complex manipulation traces. To further enhance the cross-attention, we describe a Shape-guided Gaussian mapping strategy, providing initial priors of the manipulation shape. Finally, observing that the latter manipulation in a sequence may influence traces left in the earlier one, we intriguingly invert the prediction order from forward to backward, leading to notable gains as expected. Extensive experimental results demonstrate that our method outperforms others by a large margin, highlighting the superiority of our method.

## 1 Introduction

Recent advancements in deep generative techniques have significantly improved the visual quality of generated faces. One such technique, DeepFake, allows for effortless manipulation of faces, with results that are often imperceptible to the naked eye. This technique has found applications in virtual reality and movie special effects, but it also raises severe security concerns [He *et al.*, 2021]. To address these concerns, various forensic methods have been proposed to expose DeepFakes, garnering considerable attention.

\*Corresponding author.

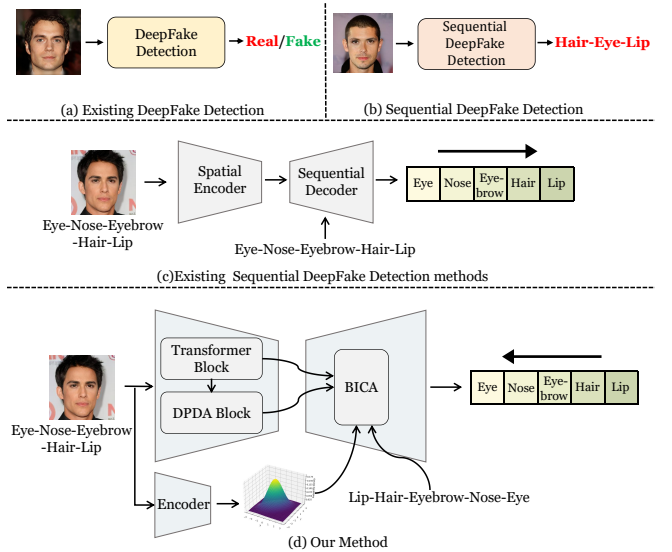


Figure 1: (a) and (b) describe the difference between conventional DeepFake detection and sequential DeepFake detection. (c) illustrates the process of classic sequential DeepFake detection methods, while (d) represents our proposed method.

Conventional forensics methods mainly focus on determining whether a given face image is authentic or forged, which typically falls into the binary classification task. However, with the rapid evolution of face editing tools, the manipulation process has become more versatile and user-friendly, enabling the use of multiple specific operations iteratively until the desired effects are reached. Under this circumstance, existing methods have limitations as they can only identify the final step of manipulation, providing limited insights into the manipulation details and hindering traceability and interpretability. To overcome this issue, a new forensics task called *Sequential DeepFake Detection* [Shao *et al.*, 2022] has emerged recently, aiming to uncover the sequences of face manipulations (see Fig. 1(a,b)). This task expands the scope of DeepFake detection and poses a new challenge to this field.

Typically, Transformer-based architectures are employed in sequential DeepFake detection to capture traces of different manipulations and predict the manipulation sequences, following the pipeline of image-to-sequence [Vinyals *et al.*, 2015]. These methods commonly employ a plain Trans-

former encoder to extract spatial clues and utilize a Transformer decoder to capture the sequential clues (see Fig. 1(c)). Despite these methods showing a certain effectiveness, many critical perspectives are lacking in further exploration.

- ♣ **Fine-grained Traces Extraction:** Generative models often exhibit imperfect semantic disentanglement. One specific manipulation may affect the entire facial structure and leave subtle traces on unintended manipulated regions. To expose the sequential manipulation, existing methods usually utilize a general Transformer encoder to capture those traces. However, this encoder concentrates on the global relationship of the entire faces and may fail to capture the subtle manipulation traces.
- ♣ **Manipulation Shape Guidance:** In the training stage, existing methods enhance the modeling of sequential relation in the decoder by estimating the scale and position of manipulation regions as priors. However, such priors are impractical as the manipulation regions are likely irregular, which could not be well described by only using the scale and position.
- ♣ **Prediction Order:** Existing methods predict the manipulation sequences in a forward order, which is the same as the actual manipulation order. However, the previous manipulation always hides beneath the subsequent manipulation. Think that it is challenging to solely take out the center of an “onion” without peeling off its skin layers. Similarly, the first manipulation is the most challenging to detect, and this challenge hinders the model from gradually capturing sequential traces.

In this paper, we delve into the above perspectives and propose a Texture-aware and Shape-guided Transformer (TSFormer) to expose sequential DeepFakes (see Fig. 1(d)). Our method introduces four major improvements, each derived from a specific perspective. 1) In the encoder, we develop two branches for capturing different types of manipulation traces. One is the vanilla branch, which is composed of conventional Transformer blocks that capture global relationships. Inspired by the effect of textures in forgery detection [Liu *et al.*, 2020; Yang *et al.*, 2021], we design a texture-aware branch to capture the subtle manipulation traces. In this branch, we describe a Diversiform Pixel Difference Attention (DPDA) module, which adaptively integrates various texture extraction operations into the self-attention mechanism, with guidance from the vanilla branch. 2) Then we propose a new Bidirectional Interaction Cross-attention (BICA) module to effectively model correlations among the spatial features from the encoder and sequential manipulation annotations. Unlike standard cross-attention, our module simultaneously processes multiple features and employs a multi-level fusion strategy for more effective correlations. 3) To enhance cross-attention, we propose a Shape-guided Gaussian Mapping strategy to provide the priors of manipulation shapes. Instead of estimating the scale and position, we predict the Gaussian distribution of their manipulated shapes using a Variational Auto-encoder (VAE). 4) Subsequently, we invert the order of the manipulation sequences in the training phase. This simple “trick” notably improves the detection performance as expected. Our method is evaluated on a pub-

lic sequential DeepFake dataset and compared with several state-of-the-art methods, demonstrating the effectiveness of our method in detecting sequential DeepFakes.

The contribution of this paper is summarized as

1. We introduce a texture-aware branch to capture subtle manipulation traces. To achieve this, we describe a Diversiform Pixel Difference Attention (DPDA) module, which adaptively integrates various texture extraction operations into the self-attention mechanism.
2. We describe a Bidirectional Interaction Cross-attention (BICA) module to effectively model the correlations among spatial and sequential features in a multi-level fusion strategy. Then we propose a Shape-guided Gaussian Mapping strategy to enhance cross-attention.
3. By intriguingly inverting the prediction order of manipulation sequences, we achieve notable performance gains.
4. Through extensive experiments, we demonstrate the efficacy of our method and thoroughly study the effect of each component of our method for further exploration.

## 2 Related Works

**DeepFake Detection.** To combat the threats posed by DeepFake, a considerable amount of methods have been proposed for DeepFake detection [Li *et al.*, 2018; Yang *et al.*, 2019; Gu *et al.*, 2022; Xu *et al.*, 2023; Dong *et al.*, 2023; Guo *et al.*, 2023; Wang *et al.*, 2023]. These methods can typically be classified into different categories in terms of the way of feature capturing. The methods of [Li *et al.*, 2018; Yang *et al.*, 2019; Agarwal *et al.*, 2019; Qi *et al.*, 2020; Yu *et al.*, 2024] expose DeepFake by capturing abnormal biological signals, such as eye blinking, behavior patterns, or heart rhythm. Other methods focus on extracting the spatial artifacts introduced either by face generation or the blending operations [Li and Lyu, 2019; Li *et al.*, 2020; Zhao *et al.*, 2021c; Shiohara and Yamasaki, 2022]. Instead of capturing the spatial artifacts, the methods of [Li *et al.*, 2021; Liu *et al.*, 2021; Dzanic *et al.*, 2020] demonstrate the effectiveness of frequency information and capture representative traces in the frequency domain. Moreover, many recent methods design dedicated models to capture the traces automatically [Zhao *et al.*, 2021a; Guo *et al.*, 2023; Wang *et al.*, 2023]. However, these methods can only predict authenticity, which can not handle and analyze the multi-step alterations in practice.

**Sequential DeepFake Detection.** Sequential DeepFake detection is proposed to predict the sequential manipulations in order. This task is generally formulated as the image-to-sequence problem and utilizes sequential-related architectures for detection. The method of [Shao *et al.*, 2022] solves this task using a plain Transformer architecture. In this paper, we further explore this task and describe a new method dedicated to sequential DeepFake detection. Our method features four major improvements and has demonstrated effectiveness in experiments.

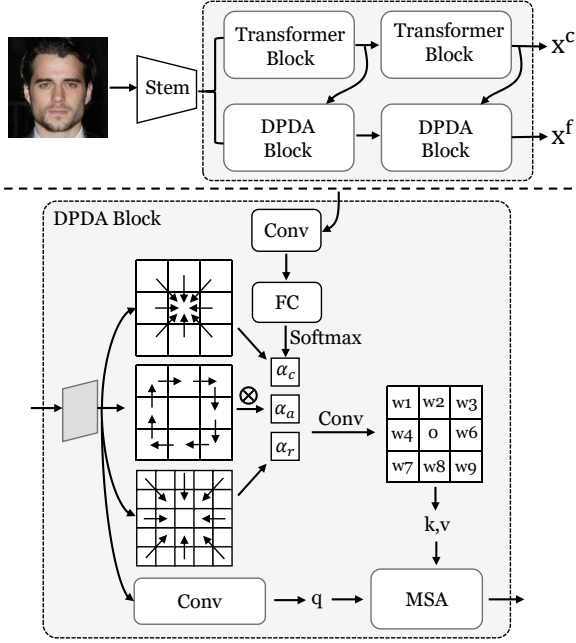


Figure 2: Overview of the spatial encoder (top). Illustration of DPDA module (bottom). MSA denotes Multi-head Self-attention.

### 3 Method

Our method consists of a Transformer encoder and a Transformer decoder. The encoder takes the face images as input and extracts spatial manipulation features, while the decoder models the sequential relation based on these features and sequence annotations to predict the facial manipulation sequence.

The encoder is composed of a vanilla branch and a new texture-aware branch. In the texture-aware branch, we introduce the Diversiform Pixel Difference Attention (DPDA) module to capture subtle manipulation traces (Sec. 3.1). For the decoder, we propose a Bidirectional Interaction Cross-attention strategy to fuse the extracted spatial features with the sequence annotation embeddings, enabling effective modeling of sequential relations (Sec. 3.2). To provide more guidance, we introduce Shape-guided Gaussian Mapping to enhance the effect of cross-attention in sequential modeling (Sec. 3.2). We then introduce the procedure for inverting the prediction orders (Sec. 3.2) and outline the overall loss functions (Sec. 3.3).

#### 3.1 Spatial Encoder

**Tokenization.** Denote a face image as  $\mathbf{I} \in \mathbb{R}^{H \times W \times 3}$ . To tokenize this face image, we employ a simple CNN stem following [He *et al.*, 2015]. Let a CNN stem be  $\mathcal{F}$ . The input tokens can be obtained as  $\mathbf{x}^0 = \mathcal{F}(\mathbf{I}) + \mathbf{p}$ ,  $\mathbf{z}^0 \in \mathbb{R}^{h \times w \times c}$ , where  $\mathcal{F}(\mathbf{I})$  is the feature maps from CNN model and  $\mathbf{p}$  is a positional embedding. Then we flatten the spatial dimension of these tokens to one dimension as the input of the encoder.

**Vanilla Branch.** This branch contains several Transformer blocks and each block calculates a multi-head self-attention. Denote the index of a block as  $l$  and the input token of this block as  $\mathbf{x}^l$ . Thus the operation of this block can be written

as

$$\begin{aligned} \hat{\mathbf{x}}^l &= \mathbf{x}^l + \text{MSA}(\text{LN}(\mathbf{x}^l)), \\ \hat{\mathbf{x}}^{l+1} &= \hat{\mathbf{x}}^l + \text{FFN}(\text{LN}(\hat{\mathbf{x}}^l)), \end{aligned} \quad (1)$$

where MSA denotes the multi-head self-attention operation, LN denotes the LayerNorm [Ba *et al.*, 2016], FFN is the feed-forward network, which consists of two FC layers with GELU [Hendrycks and Gimpel, 2016].

Let  $\mathbf{x}$  be the input tokens of MSA layer. In each head, three projection matrices are applied to generate query, key, and value features. Then the self-attention is conducted over the input tokens spatially to learn the coarse-grained traces. Within the  $i$ -th head, the self-attention can be defined as

$$\begin{aligned} Q_i &= \mathbf{x}W_i^Q, K_i = \mathbf{x}W_i^K, V_i = \mathbf{x}W_i^V, \\ h_i &= \text{Softmax}(Q_iK_i^\top / \sqrt{d_i})V_i, \\ \text{MSA}(\mathbf{x}) &= \text{Concat}(h_1, \dots, h_n)W^o, \end{aligned} \quad (2)$$

where  $W_i^Q, W_i^K, W_i^V$  are the projection matrices,  $d_i$  is the number of hidden dimensions, and  $h_i$  is the self-attention of  $i$ -th head. Then we concatenate all these heads and perform a linear transformation with  $W^o$  to obtain the final output.

**Texture-aware Branch.** To extract these subtle manipulation traces, we develop a new Transformer block designed specifically for extracting texture features. Our block draws inspiration from central difference operators [Yu *et al.*, 2020b; Juefei-Xu *et al.*, 2017], which are convolutions used for detecting local textures. In our method, we derive and extend their essence from the convolution style to the self-attention mechanism, and propose a Diversiform Pixel Difference Attention (DPDA) module that captures fine-grained spatial traces while retaining the global view within the vanilla self-attention.

1) *Revisit of Central Difference Convolution.* Central difference convolution is a special case of convolution, which emphasizes the center-oriented gradients in the local receptive field region. Given a feature map  $\mathbf{x}$ , this operation can be formulated as

$$\mathbf{x}'(p_0) = \sum_{p_n \in \mathcal{O}} \mathbf{w}(p_n) \cdot (\mathbf{x}(p_0 + p_n) - \mathbf{x}(p_0)), \quad (3)$$

where  $\mathbf{w}$  is the convolution kernel,  $\mathcal{O}$  denotes the local receptive field,  $p_0$  indicates the current location of input feature map  $\mathbf{x}$  and output feature map  $\mathbf{x}'$ , and  $p_n$  is the relative position in  $\mathcal{O}$ .

2) *Diversiform Pixel Difference Attention.* Inspired by the central difference operations, we extend these operations and integrate such spirit into the self-attention mechanism following [Yu *et al.*, 2020b; Yu *et al.*, 2020a; Miao *et al.*, 2023]. Specifically, given the feature map  $\mathbf{x}$ , we first perform a vanilla convolution on it to generate the query feature, which is defined as

$$\mathbf{x}^Q(p_0) = \sum_{p_n \in \mathcal{O}} \mathbf{w}(p_n) \cdot \mathbf{x}(p_0 + p_n). \quad (4)$$

Then we would like to capture the fine-grained spatial features as the source of key and value features. Since the central difference operations focus on the center-oriented gradients, they may overlook other texture patterns, which hinders

the effectiveness of capturing manipulation traces. To obtain a diverse range of gradient information, we leverage the concept of Extended Local Binary Pattern (ELBP), which can encode the pixel relations from various perspectives, including central, angular, and radial directions [Su *et al.*, 2021]. The angular direction calculates the difference between adjacent pixels in the outline of the kernel in a certain order, while the radial direction calculates the difference between radial adjacent pixels, see Fig. 2. To obtain the key and value features, we adaptively ensemble these operations using a learnable coefficient vector, which is formulated as

$$\begin{aligned} \mathbf{x}^{K,V}(p_0) &= \sum_{p_n \in \mathcal{O}} \mathbf{w}(p_n) \cdot \left( \alpha_c \cdot \underbrace{(\mathbf{x}(p_0 + p_n) - \mathbf{x}(p_0))}_{\mathcal{D}_c} \right. \\ &\quad + \alpha_a \cdot \underbrace{(\mathbf{x}(p_0 + p_n) - \mathbf{x}(p_{n-1}))}_{\mathcal{D}_a} \\ &\quad \left. + \alpha_r \cdot \underbrace{(\mathbf{x}(p_0 + p_n) - \mathbf{x}(p_{\phi(n)}))}_{\mathcal{D}_r} \right) \\ &= \sum_{p_n \in \mathcal{O}} \mathbf{w}(p_n) \cdot \left( \underbrace{[\alpha_c, \alpha_a, \alpha_r]}_{\boldsymbol{\alpha}} \begin{bmatrix} \mathcal{D}_c \\ \mathcal{D}_a \\ \mathcal{D}_r \end{bmatrix} \right). \end{aligned} \quad (5)$$

In this equation,  $\mathcal{D}_c, \mathcal{D}_a, \mathcal{D}_r$  denote central, angular, and radial difference operations respectively. We use  $3 \times 3$  as the local receptive field  $\mathcal{O}$  for instance and set  $\mathcal{O} = \{(-1, -1), (-1, 0), \dots, (1, 1)\}$ . Thus  $\phi(n)$  in radial difference operation can be defined as  $\phi(n) = (2x, 2y)$  if  $n = (x, y)$ .  $\boldsymbol{\alpha}$  is the coefficient vector to balance the contribution of each operation.

Given that different DeepFake face images may contain different manipulation traces, we design a learning scheme to adaptively balance the contribution strength of different DPDA operations. As our first branch concentrates on extracting coarse-grained information, its intermediate features can provide global instruction on the composition of manipulations. Denote the feature map of the corresponding block in our coarse-grained branch as  $\mathbf{x}^l$ . To achieve this adaptive learning, we design a sub-network  $\mathcal{H}$  that contains several convolution layers. This network learns the  $\boldsymbol{\alpha}$  based on  $\mathbf{x}^l$  as

$$\boldsymbol{\alpha} = \text{Softmax}(\mathcal{H}(\mathbf{x}^l)). \quad (6)$$

After obtaining  $\mathbf{x}^Q$  and  $\mathbf{x}^{K,V}$ , we project the query feature  $\mathbf{x}^Q$  into query tokens, and project  $\mathbf{x}^{K,V}$  into key and value tokens. Within each head,  $Q_i = \mathbf{x}^Q W_i^Q, K_i = \mathbf{x}^{K,V} W_i^K, V_i = \mathbf{x}^{K,V} W_i^V$ . Then the multi-head self-attention is calculated using the Eq. (2).

3) *Diversiform Pixel Difference Transformer Block.* This block integrates the Diversiform Pixel Difference Attention (DPDA) module, which is similar to the Eq. (1). The overall process can be written as

$$\begin{aligned} \hat{\mathbf{x}}^l &= \mathbf{x}^l + \text{DPDA}(\text{LN}(\mathbf{x}^l)), \\ \hat{\mathbf{x}}^{l+1} &= \hat{\mathbf{x}}^l + \text{FFN}(\text{LN}(\hat{\mathbf{x}}^l)), \end{aligned} \quad (7)$$

With this strategy, this branch can effectively extract subtle manipulation traces, enhancing the performance in sequential detection.

### 3.2 Sequential Decoder

In order to predict sequential manipulations, we develop a sequential decoder architecture, which takes as input the features from the encoder and the embeddings of manipulation sequences. To effectively integrate these types of features into the decoder, we propose a Bidirectional Interactive Cross-attention (BICA) strategy that can properly integrate the features from the encoder into the decoder. Moreover, to improve the capacity of cross-attention, we introduce a shape-guided Gaussian mapping strategy to enhance its effectiveness.

**Spatial and Sequential Feature Fusing.** To fully leverage the benefits of both coarse-grained and fine-grained features, we propose a Bidirectional Interaction Cross-attention (BICA) module. This module employs a hierarchical attention mechanism to explore the correlation between features and sequential annotations.

1) *Revisit of Conventional Cross-attention* The cross-attention is typically employed in the decoder of the transformer for sequence tasks. Unlike self-attention mechanisms, the query, and key and value features usually originate from different sources. Given two input tokens from different sources  $\mathbf{x}_1$  and  $\mathbf{x}_2$ , the multi-head cross-attention (MCA) can be defined as

$$\begin{aligned} Q_i &= \mathbf{x}_1 W_i^Q, K_i = \mathbf{x}_2 W_i^K, V_i = \mathbf{x}_2 W_i^V, \\ h_i &= \text{Softmax}(Q_i K_i^T / \sqrt{d_i}) V_i, \\ \text{MCA}(\mathbf{x}_1, \mathbf{x}_2, \mathbf{x}_2) &= \text{Concat}(h_1, \dots, h_n) W^o, \end{aligned} \quad (8)$$

2) *Bidirectional Interactive Cross-attention.* Let  $\mathbf{x}^c$  and  $\mathbf{x}^f$  represent the features from the coarse-grained and fine-grained branches. Let  $\mathbf{x}^s$  be the embedding of sequential manipulation annotations. In our task, it is intuitive to perform separate MCA operations on  $\mathbf{x}^s$  with  $\mathbf{x}^c$  and  $\mathbf{x}^f$ . However, this integration fails to explore deeper connections between these three features. Inspired by the concept of multi-modal cross-attentions [Yu *et al.*, 2019; Wei *et al.*, 2020; Zhang *et al.*, 2023], we propose Bidirectional Interactive Cross-attention (BICA) which employs a multi-level fusion strategy to fully excavate the underlying correlations. The overview of this module is shown in Fig. 3.

Firstly, we perform MSA on  $\mathbf{x}^s$  to find the correlations of sequential manipulation annotations, which is then subjected to MCA with  $\mathbf{x}^c$  and  $\mathbf{x}^f$  to build the cross-attention. Then these processed features are summed up and applied Layer-Norm to generate multi-modal features  $\mathbf{a}^c$  and  $\mathbf{a}^f$ . These operations can be written as

$$\begin{aligned} \tilde{\mathbf{x}}^s &= \text{MSA}(\mathbf{x}^s), \\ \tilde{\mathbf{a}}^c &= \text{MCA}(\tilde{\mathbf{x}}^s, \mathbf{x}^c, \mathbf{x}^c), \mathbf{a}^c = \text{LN}(\tilde{\mathbf{a}}^c + \tilde{\mathbf{x}}^s), \\ \tilde{\mathbf{a}}^f &= \text{MCA}(\tilde{\mathbf{x}}^s, \mathbf{x}^f, \mathbf{x}^f), \mathbf{a}^f = \text{LN}(\tilde{\mathbf{a}}^f + \tilde{\mathbf{x}}^s). \end{aligned} \quad (9)$$

We then perform interactive cross-attention between features of  $\mathbf{a}^c$  and  $\mathbf{a}^f$  in two directions as

$$\begin{aligned} \tilde{\mathbf{a}}^{c,f} &= \text{MCA}(\mathbf{a}^c, \mathbf{a}^f, \mathbf{a}^f), \mathbf{a}^{c,f} = \text{LN}(\tilde{\mathbf{a}}^{c,f} + \mathbf{a}^c), \\ \tilde{\mathbf{a}}^{f,c} &= \text{MCA}(\mathbf{a}^f, \mathbf{a}^c, \mathbf{a}^c), \mathbf{a}^{f,c} = \text{LN}(\tilde{\mathbf{a}}^{f,c} + \mathbf{a}^f). \end{aligned} \quad (10)$$

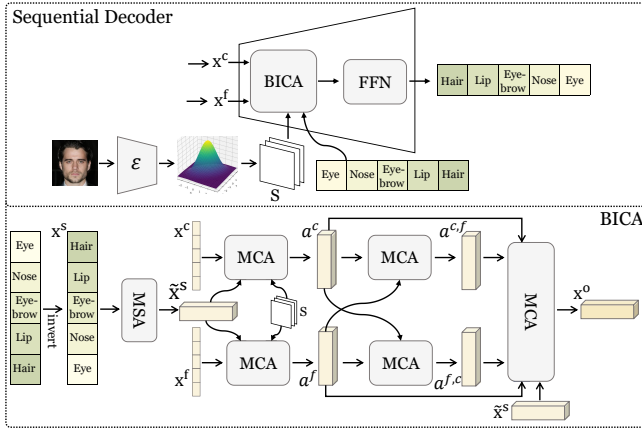


Figure 3: Overview of the sequential decoder (top). Illustration of Bidirectional Interactive Cross-attention (BICA). MCA denotes Multi-head Cross-attention.

Next, we fuse the sequential features  $\tilde{\mathbf{x}}^s$  with the enhanced spatial features  $\mathbf{a}^{c,f}$  and  $\mathbf{a}^{f,c}$ , following the operations as

$$\begin{aligned} \mathbf{A} &= [\mathbf{a}^c, \mathbf{a}^f, \mathbf{a}^{c,f}, \mathbf{a}^{f,c}], \\ \tilde{\mathbf{x}}^o &= \text{MCA}(\tilde{\mathbf{x}}^s, \mathbf{A}, \mathbf{A}), \\ \mathbf{x}^o &= \text{LN}(\tilde{\mathbf{x}}^o + \tilde{\mathbf{x}}^s). \end{aligned} \quad (11)$$

Through this fusion strategy, the sequential and spatial features can be fully interacted with and expose the underlying correlations.

**Shape-guided Gaussian Mapping** In comparison to general image-sequence tasks, sequential manipulation annotations in our case are relatively short and may not provide sufficient guidance. To address this limitation, we propose a Shape-guided Gaussian Mapping strategy to leverage the strong spatial position priors associated with each manipulation component in the faces. Specifically, we assume that the position of each facial manipulation follows a Gaussian distribution. By learning these distributions, we can determine the probability of each position on a face image being manipulated. To simulate these Gaussian distributions, we construct a Variational Auto-encoder (VAE) [Kingma and Welling, 2013] with the image  $\mathbf{I}$  as input. The VAE architecture contains an encoder  $\mathcal{E}$  and a decoder  $\mathcal{D}$ . The encoder transforms the input feature into means  $\boldsymbol{\mu}$  and standards  $\boldsymbol{\sigma}$  of these Gaussian distributions, while the decoder reconstructs the input images from the sampled latent code. Through the reconstruction process, the encoder learns to capture the spatial manipulation information and formulate them as Gaussian distributions. Next, we create a grid map  $M$  that is composed of the  $x$ - and  $y$ -coordinates of each position. This grid map is then used to predict the probability of each position in different facial manipulations. These operations can be formulated as

$$\begin{aligned} \boldsymbol{\mu}, \boldsymbol{\sigma} &= \mathcal{E}(\mathbf{I}), \\ S &= \mathcal{N}(M | \boldsymbol{\mu}, \boldsymbol{\sigma}), \end{aligned} \quad (12)$$

where  $S$  is the probability map for each spatial position. This map is integrated into the MCA operations  $\text{MCA}(\tilde{\mathbf{x}}^s, \mathbf{x}^c, \mathbf{x}^c)$  and  $\text{MCA}(\tilde{\mathbf{x}}^s, \mathbf{x}^f, \mathbf{x}^f)$  in Eq. (9) respectively. We take the

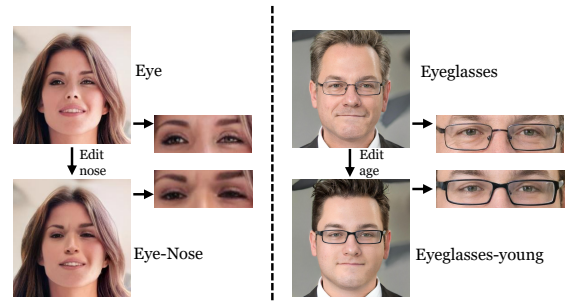


Figure 4: The impact of the sequential manipulation on facial attributes. The second manipulation impacts the first manipulation on (left) eye and (right) eyeglasses.

integration in  $\text{MCA}(\tilde{\mathbf{x}}^s, \mathbf{x}^c, \mathbf{x}^c)$  for example as

$$\begin{aligned} Q_i &= \tilde{\mathbf{x}}^s W_i^Q, K_i = \mathbf{x}^c W_i^K, V_i = \mathbf{x}^c W_i^V, \\ h_i &= \text{Softmax}(Q_i K_i^T / \sqrt{d_i} + \eta \cdot S) V_i, \\ \text{MCA}(\tilde{\mathbf{x}}^s, \mathbf{x}^c, \mathbf{x}^c) &= \text{Concat}(h_1, \dots, h_n) W^o. \end{aligned} \quad (13)$$

By inserting the shape priors of facial manipulation, the cross-attention is greatly enhanced to capture the spatial and sequential forgery traces.

**Inverted Order Prediction.** Based on our analysis, we invert the annotation of the manipulation sequence for training. For instance, given a manipulated face with annotation of “eyes-nose-eyebrow-lips-hair”, we reorder it as “hair-lips-eyebrow-nose-eyes”, and convert it to  $\mathbf{x}^s$  for sequential modeling. By doing so, the model first predicts the last manipulation of “hair”. By isolating the disturbance caused by “hair”, the model can then focus on predicting the next manipulation, which is “lips”. The rationale behind this strategy is that the manipulation of the nose can affect the manipulation of the eyes, making the detection of eye manipulations more challenging. On the other hand, the manipulation in hair is not influenced by other manipulations, making it more easily detectable (see Fig. 4). The advantage of this strategy is that, compared to forward sequence predictions, each step in the inverted sequence predictions is only influenced by itself and is independent of other types of manipulations.

### 3.3 Loss Function

In the training phase, we employ an auto-regressive mechanism [Graves, 2013] to model sequence relationships with the cross-entropy loss  $L_{ce}$ . This loss measures the error of predicted manipulation sequence and ground truth. For the shape-guided module, we perform the general image reconstruction loss  $L_{rec}$  and KLD loss  $L_{kld}$  used in VAE [Kingma and Welling, 2013]. The overall loss function is expressed as

$$L = L_{ce} + \lambda_1 L_{rec} + \lambda_2 L_{kld}, \quad (14)$$

where  $\lambda_1, \lambda_2$  are weights for balancing these loss terms.

## 4 Experiments

### 4.1 Experimental Settings

**Datasets.** Our experiments are conducted on Sequential DeepFake Dataset (SDD) [Shao *et al.*, 2022]. This dataset

Table 1: Performance of different methods on detecting sequential DeepFakes.

Methods	Facial-components		Facial-attributes		Average	
	Fixed-Acc	Adaptive-Acc	Fixed-Acc	Adaptive-Acc	Fixed-Acc	Adaptive-Acc
Multi-Cls (ResNet-34)	69.66	50.54	66.99	46.68	68.33	48.61
Multi-Cls (ResNet-50)	69.65	50.57	66.66	46.00	68.16	48.29
DETR (ResNet-34)	69.87	50.63	67.93	48.15	68.90	49.39
DETR (ResNet-50)	69.75	49.84	67.62	47.99	68.69	48.92
DRN (ResNet-34)	66.06	45.79	64.42	43.20	65.24	44.50
MA (ResNet-34)	71.31	52.94	67.58	47.48	66.45	50.21
Two-Stream (ResNet-34)	71.92	53.89	66.77	46.38	69.35	50.14
SeqFake-Former (ResNet-34)	70.88	52.96	67.85	48.36	69.37	50.66
SeqFake-Former (ResNet-50)	69.41	50.22	68.38	48.97	68.90	49.60
<b>TS-Former (Ours) (ResNet-34)</b>	<b>74.70</b>	<b>58.43</b>	<b>69.13</b>	<b>49.68</b>	<b>71.92</b>	<b>54.06</b>
<b>TS-Former (Ours) (ResNet-50)</b>	<b>73.32</b>	<b>56.08</b>	<b>68.86</b>	<b>49.67</b>	<b>71.09</b>	<b>52.88</b>

Table 2: Ablation study on the facial-components datasets.

Setting	Resnet-34		Resnet-50	
	Fixed-Acc	Adaptive-Acc	Fixed-Acc	Adaptive-ACC
Baseline	69.65 (+0.00)	50.43 (+0.00)	68.84 (+0.00)	49.40 (+0.00)
Baseline+DPDA	70.24 (+0.59)	51.87 (+1.44)	69.23 (+0.39)	51.05 (+1.65)
Baseline+DPDA+BICA	71.00 (+1.35)	52.67 (+2.24)	71.55 (+2.71)	53.06 (+3.66)
Baseline+DPDA+BICA+IOP	73.32 (+3.67)	56.65 (+6.22)	72.65 (+3.81)	55.03 (+5.63)
Baseline+DPDA+BICA+IOP+SGM	<b>74.70 (+5.05)</b>	<b>58.43 (+8.00)</b>	<b>73.32 (+4.48)</b>	<b>56.08 (+6.68)</b>

contains two types of sequential DeepFake manipulations, the facial components manipulation and the facial attributes manipulation. The first track comprises 35, 166 face images that are subjected to replacing operations on specific facial components. There are 28 manipulation types in this track, with a maximum sequence length of five. The second track contains 49, 920 face images with 26 types of attribute manipulations. The maximum length of each manipulation is also five. Its split of training, validating, and testing set is 8 : 1 : 1.

**Evaluation Metrics.** In line with previous work [Shao *et al.*, 2022], we employ Fixed Accuracy (Fixed-Acc) and Adaptive Accuracy (Adaptive-Acc) for evaluation. To calculate the Fixed-Acc score, the sequence annotations shorter than five are padded with the label “no manipulation” and then compare the predictions with the padded sequence annotation. On the other hand, due to the nature of the auto-regress mechanism, the model can stop predicting upon encountering the End-of-Sequence (EOS) symbol, resulting in various lengths of the predicted sequence. The adaptive-Acc score is calculated by comparing the predictions with the sequence annotations in terms of dynamic lengths.

**Implementation Details.** We utilize ResNet-34 [He *et al.*, 2015] as our CNN stem in main experiment. Each branch in the spatial encoder has two Transformer blocks. Each block contains four attention heads. The sequential decoder consists of two Transformer blocks. In the training phase, the image size is set to  $256 \times 256$  with augmentations such as horizontal Flipping and adjusting the brightness of the image. We employ the AdamW optimizer with a weight decay of  $10^{-4}$ . The initial learning rates are set to  $10^{-4}$  for CNN stem and  $10^{-4}$  for Transformer architecture. We utilize a warm-up strategy of 20 epochs, with a batch size of 32. The total epochs are set to 170, with a 10% reduction in learning rate every 50 epochs. The parameters in the loss function are set as:  $\lambda_1 = 0.1, \lambda_2 = 0.01$ .

## 4.2 Results

Table 1 shows the performance of our method compared to other counterparts, including Multi-Cls, DETR [Carion *et al.*, 2020], DRN [Wang *et al.*, 2019], MA [Zhao *et al.*, 2021b], Two-Stream [Luo *et al.*, 2021], SeqFake-Former [Shao *et al.*, 2022] respectively. Multi-Cls and DETR serve as baseline methods adapted from models for general vision tasks. Multi-Cls performs multi-label classification by directly classifying the manipulated images into multiple classes. DETR is a modified object detector that replaces object queries with manipulation annotation. DRN, MA, and Two-Stream are DeepFake detection methods adapted by substituting the binary classification head with a multi-classification head. These methods are all referenced from [Shao *et al.*, 2022]. SeqFake-Former is a recent dedicated method for sequential DeepFake detection. We reproduce this method rigorously using their release codes. As shown in Table 1, our method outperforms baseline methods by a large margin, averaging 71.92% and 54.06% in Fixed-Acc and Adaptive-Acc scores, respectively. Moreover, our method surpasses the DeepFake detection methods in both tracks. Notably, compared to SeqFakeFormer, our method achieves improvements by 3.82%, 5.47% and 1.28%, 1.32% in these two tracks.

The results also indicate that all methods perform better in Fixed-Acc than in Adaptive-Acc. This observation is consistent with the findings in [Shao *et al.*, 2022] that predicting manipulation sequences with varying lengths is a more challenging task. In real-world applications, manipulation sequences with varying lengths are more practical, thus the improvement of our method in this metric sufficiently represents the practicability of the proposed modules.

Intriguingly, we observe that ResNet-50 performs slightly worse than ResNet-34 across all methods. This contrasts with the expectation that a larger model should have stronger capacity. We discuss this phenomenon in Sec. 4.4.

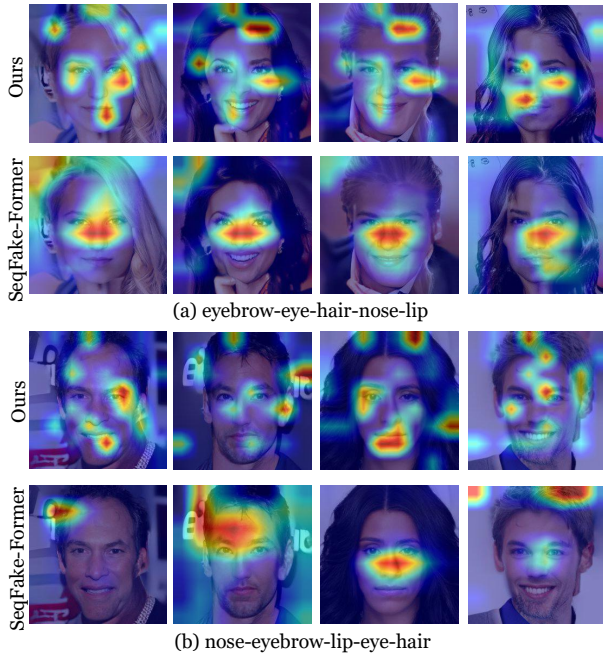


Figure 5: The visualization of our model and SeqFakeFormer under the (a) eyebrow-eye-hair-nose-lip and (b) nose-eyebrow-lip-eye-hair manipulating annotations.

### 4.3 Ablation Study

Our method consists of several key components, including the Diversified Pixel Difference Attention module (DPDA), Bidirectional Interactive Cross-attention (BICA), Inverted Order Prediction (IOP), and Shape-guided Gaussian Mapping (SGM). To evaluate the effectiveness of each component, we conduct a series of ablation studies on the facial-components track using the stem of ResNet-34 and ResNet-50.

Specifically, we designed different models based on the following settings: **1)** A baseline model with a Transformer architecture that only consists of basic encoders and decoders. **2)** Adding the DPDA module to the baseline model, which generates two spatial features from the encoder. Then we directly add these two features and feed them into the sequential decoder. **3)** Adopting the BICA strategy on the baseline model for feature integration. **4)** Incorporating inverted order prediction. **5)** Inserting the SGM module into BICA strategy.

The results of the ablation studies are shown in Table 2. It can be observed that each component contributes to the overall performance. Taking Resnet-34 as an example. The DPDA module improves the Fixed-Acc and Adaptive-Acc by 0.59% and 1.44%, respectively. The BICA strategy further enhances the performance by 0.76% and 0.8% in Fixed-Acc and Adaptive-Acc. After applying IOP, the performance is significantly improved by 2.32% in Fixed-Acc and 3.98% in Adaptive-Acc, showing the effectiveness of this strategy in gradually capturing manipulation traces. Finally, the integration of SGM yields further performance, achieving the best performance when all components are applied.

### 4.4 Discussion

**Attention Visualization.** To assess the learning ability of our method, we visualize the attention maps of our method com-

Table 3: Performance on Different CNN Stems.

Stem	Fixed-Acc		Adaptive-Acc	
	SFF	Ours	SFF	Ours
ResNet-18	68.41	69.97	49.55	52.26
ResNet-34	70.88	74.70	52.96	58.43
Resnet-50	69.41	73.32	50.22	56.08
Resnet-101	68.87	73.46	49.06	56.77

pared with Seq-FakeFormer under two different manipulation annotations, eyebrow-eye-hair-nose-lip and nose-eyebrow-lip-eye-hair. Fig. 5 shows the Grad-CAM [Selvaraju *et al.*, 2019] of these methods. We observe that under the same annotation, our method can identify the manipulated regions more precisely. In contrast, Seq-FakeFormer can localize the major manipulated regions but may overlook small manipulations with subtle traces. This result highlights the effectiveness of our method in capturing sequential manipulation traces.

Furthermore, we also observe that our method can highlight regions that are not annotated as manipulation. We attribute this to the imperfect nature of GAN in the feature space, causing subtle influences on some neighboring areas during the multi-step facial manipulation process. Our method can capture this subtle alternation as evidence for exposing the sequential manipulations.

### Controversy Regarding CNN Stem.

From Table 3 we observe an unexpected phenomenon where using ResNet-34 as CNN stem achieves better performance than ResNet-50. To further investigate this, we validate our method using ResNet-18 and ResNet-101. Table 3 shows the performance comparison of our method and SeqFake-Former (SFF) on these architectures. It can be seen that the performance of ResNet-18 is notably degraded compared to ResNet-34, aligning with our expectations. However, when using ResNet-101 as the Stem, it yields lower performance than ResNet-50. This finding contradicts the general understanding that increasing the model size and parameters can improve feature extraction capacity. One possible explanation for this phenomenon is that the length of the manipulation sequence is relatively short (less than five), which increases the likelihood of overfitting in large models. This suggests the need to strike a balance between model size and performance in the future.

## 5 Conclusion

We introduce a novel Texture-aware and Shape-guided Transformer to enhance detection performance. Compared to the classic Transformer-based methods, we introduce four improvements. Firstly, we describe a new Diversiform Pixel Difference Attention module (DPDA) to capture subtle manipulation traces. Moreover, we introduce a Bidirectional Interaction Cross-attention module (BICA) to explore deep correlations between spatial and sequential features. To further enhance the cross-attention, we describe a Shape-guided Gaussian mapping strategy to provide the priors of manipulation shapes. Lastly, we improve the performance by inverting the prediction order from forward to backward. The results obtained on public datasets demonstrate the efficacy of our method in sequential DeepFake detection.

## References

- [Agarwal *et al.*, 2019] Shruti Agarwal, Hany Farid, Yuming Gu, Mingming He, Koki Nagano, and Hao Li. Protecting world leaders against deep fakes. In *IEEE Conference on Computer Vision and Pattern Recognition Workshops (CVPRW)*, 2019.
- [Ba *et al.*, 2016] Jimmy Lei Ba, Jamie Ryan Kiros, and Geoffrey E Hinton. Layer normalization. *arXiv preprint arXiv:1607.06450*, 2016.
- [Carion *et al.*, 2020] Nicolas Carion, Francisco Massa, Gabriel Synnaeve, Nicolas Usunier, Alexander Kirillov, and Sergey Zagoruyko. End-to-end object detection with transformers. In *ECCV*, 2020.
- [Dong *et al.*, 2023] Shichao Dong, Jin Wang, Renhe Ji, Jiajun Liang, Haoqiang Fan, and Zheng Ge. Implicit identity leakage: The stumbling block to improving deepfake detection generalization. In *CVPR*, 2023.
- [Dzanic *et al.*, 2020] Tarik Dzanic, Karan Shah, and Freddie Witherden. Fourier spectrum discrepancies in deep network generated images. *Advances in neural information processing systems*, 33:3022–3032, 2020.
- [Graves, 2013] Alex Graves. Generating sequences with recurrent neural networks. *arXiv preprint arXiv:1308.0850*, 2013.
- [Gu *et al.*, 2022] Zhihao Gu, Taiping Yao, Yang Chen, Ran Yi, Shouhong Ding, and Lizhuang Ma. Region-aware temporal inconsistency learning for deepfake video detection. In *IJCAI*, 2022.
- [Guo *et al.*, 2023] Ying Guo, Cheng Zhen, and Pengfei Yan. Controllable guide-space for generalizable face forgery detection. In *Proceedings of the IEEE/CVF International Conference on Computer Vision*, pages 20818–20827, 2023.
- [He *et al.*, 2015] Kaiming He, Xiangyu Zhang, Shaoqing Ren, and Jian Sun. Deep residual learning for image recognition. *arXiv preprint arXiv:1512.03385*, 2015.
- [He *et al.*, 2021] Yang He, Ning Yu, Margret Keuper, and Mario Fritz. Beyond the spectrum: Detecting deepfakes via re-synthesis. In *30th International Joint Conference on Artificial Intelligence (IJCAI)*, 2021.
- [Hendrycks and Gimpel, 2016] Dan Hendrycks and Kevin Gimpel. Gaussian error linear units (gelus). *arXiv preprint arXiv:1606.08415*, 2016.
- [Juefei-Xu *et al.*, 2017] Felix Juefei-Xu, Vishnu Naresh Boddeti, and Marios Savvides. Local binary convolutional neural networks. In *IEEE Computer Vision and Pattern Recognition (CVPR)*, July 2017.
- [Kingma and Welling, 2013] Diederik P Kingma and Max Welling. Auto-encoding variational bayes. *arXiv preprint arXiv:1312.6114*, 2013.
- [Li and Lyu, 2019] Yuezun Li and Siwei Lyu. Exposing deepfake videos by detecting face warping artifacts. In *IEEE Conference on Computer Vision and Pattern Recognition (CVPR) Workshops*, 2019.
- [Li *et al.*, 2018] Yuezun Li, Ming-Ching Chang, and Siwei Lyu. In icu oculi: Exposing ai created fake videos by detecting eye blinking. In *2018 IEEE International workshop on information forensics and security (WIFS)*, pages 1–7. IEEE, 2018.
- [Li *et al.*, 2020] Lingzhi Li, Jianmin Bao, Ting Zhang, Hao Yang, Dong Chen, Fang Wen, and Baining Guo. Face x-ray for more general face forgery detection. In *Proceedings of the IEEE/CVF conference on computer vision and pattern recognition*, pages 5001–5010, 2020.
- [Li *et al.*, 2021] Jiaming Li, Hongtao Xie, Jiahong Li, Zhongyuan Wang, and Yongdong Zhang. Frequency-aware discriminative feature learning supervised by single-center loss for face forgery detection. In *Proceedings of the IEEE/CVF conference on computer vision and pattern recognition*, pages 6458–6467, 2021.
- [Liu *et al.*, 2020] Zhengzhe Liu, Xiaojuan Qi, and Philip HS Torr. Global texture enhancement for fake face detection in the wild. In *Proceedings of the IEEE/CVF conference on computer vision and pattern recognition*, pages 8060–8069, 2020.
- [Liu *et al.*, 2021] Honggu Liu, Xiaodan Li, Wenbo Zhou, Yuefeng Chen, Yuan He, Hui Xue, Weiming Zhang, and Nenghai Yu. Spatial-Phase Shallow Learning: Rethinking Face Forgery Detection in Frequency Domain. In *IEEE Conference on Computer Vision and Pattern Recognition (CVPR)*, pages 772–781, 2021.
- [Luo *et al.*, 2021] Yuchen Luo, Yong Zhang and Junchi Yan, and Wei Liu. Generalizing face forgery detection with high-frequency features. In *CVPR*, 2021.
- [Miao *et al.*, 2023] Changtao Miao, Zichang Tan, Qi Chu, Huan Liu, Honggang Hu, and Nenghai Yu. F 2 trans: High-frequency fine-grained transformer for face forgery detection. *IEEE Transactions on Information Forensics and Security*, 18:1039–1051, 2023.
- [Qi *et al.*, 2020] Hua Qi, Qing Guo, Felix Juefei-Xu, Xiaofei Xie, Lei Ma, Wei Feng, Yang Liu, and Jianjun Zhao. Deep-rhythm: Exposing deepfakes with attentional visual heart-beat rhythms. In *Proceedings of the 28th ACM international conference on multimedia*, pages 4318–4327, 2020.
- [Selvaraju *et al.*, 2019] Ramprasaath R. Selvaraju, Michael Cogswell, Abhishek Das, Ramakrishna Vedantam, Devi Parikh, and Dhruv Batra. Grad-cam: Visual explanations from deep networks via gradient-based localization. In *IJCV*, 2019.
- [Shao *et al.*, 2022] Rui Shao, Tianxing Wu, and Ziwei Liu. Detecting and recovering sequential deepfake manipulation. In *European Conference on Computer Vision (ECCV)*, 2022.
- [Shiohara and Yamasaki, 2022] Kaede Shiohara and Toshihiko Yamasaki. Detecting deepfakes with self-blended images. In *Proceedings of the IEEE/CVF Conference on Computer Vision and Pattern Recognition*, pages 18720–18729, 2022.

- [Su *et al.*, 2021] Zhuo Su, Wenzhe Liu, Zitong Yu, Dewen Hu, Qing Liao, Qi Tian, Matti Pietikainen, and Li Liu. Pixel difference networks for efficient edge detection. In *ICCV*, 2021.
- [Vinyals *et al.*, 2015] Oriol Vinyals, Alexander Toshev, Samy Bengio, and Dumitru Erhan. Show and tell: a neural image caption generator. In *CVPR*, 2015.
- [Wang *et al.*, 2019] Sheng-Yu Wang, Oliver Wang, Andrew Owens, Richard Zhang, and Alexei A. Efros. Detecting photoshopped faces by scripting photoshop. In *CVPR*, 2019.
- [Wang *et al.*, 2023] Yuan Wang, Kun Yu, Chen Chen, Xiyuan Hu, and Silong Peng. Dynamic graph learning with content-guided spatial-frequency relation reasoning for deepfake detection. In *Proceedings of the IEEE/CVF Conference on Computer Vision and Pattern Recognition*, pages 7278–7287, 2023.
- [Wei *et al.*, 2020] Xi Wei, Tianzhu Zhang, Yan Li, Yongdong Zhang, and Feng Wu. Multi-modality cross attention network for image and sentence matching. In *Proceedings of the IEEE/CVF conference on computer vision and pattern recognition*, pages 10941–10950, 2020.
- [Xu *et al.*, 2023] Yuting Xu, Jian Liang, Gengyun Jia, Ziming Yang, Yanhao Zhang, and Ran He. Tall: Thumbnail layout for deepfake video detection. In *ICCV*, 2023.
- [Yang *et al.*, 2019] Xin Yang, Yuezun Li, and Siwei Lyu. Exposing deep fakes using inconsistent head poses. In *ICASSP 2019-2019 IEEE International Conference on Acoustics, Speech and Signal Processing (ICASSP)*, pages 8261–8265. IEEE, 2019.
- [Yang *et al.*, 2021] Jiachen Yang, Aiyun Li, Shuai Xiao, Wen Lu, and Xinbo Gao. Mtd-net: learning to detect deepfakes images by multi-scale texture difference. *IEEE Transactions on Information Forensics and Security*, 16:4234–4245, 2021.
- [Yu *et al.*, 2019] Jun Yu, Jing Li, Zhou Yu, and Qingming Huang. Multimodal transformer with multi-view visual representation for image captioning. *IEEE transactions on circuits and systems for video technology*, 30(12):4467–4480, 2019.
- [Yu *et al.*, 2020a] Zitong Yu, Jun Wan, Yunxiao Qin, Xiaobai Li, Stan Z Li, and Guoying Zhao. Nas-fas: Static-dynamic central difference network search for face anti-spoofing. *IEEE transactions on pattern analysis and machine intelligence*, 43(9):3005–3023, 2020.
- [Yu *et al.*, 2020b] Zitong Yu, Chenxu Zhao, Zezheng Wang, Yunxiao Qin, Zhuo Su, Xiaobai Li, Feng Zhou, and Guoying Zhao. Searching central difference convolutional networks for face anti-spoofing. In *CVPR*, 2020.
- [Yu *et al.*, 2024] Zitong Yu, Rizhao Cai, Zhi Li, Wenhan Yang, Jingang Shi, and Alex C Kot. Benchmarking joint face spoofing and forgery detection with visual and physiological cues. *IEEE Transactions on Dependable and Secure Computing*, 2024.
- [Zhang *et al.*, 2023] Jing Zhang, Yingshuai Xie, Weichao Ding, and Zhe Wang. Cross on cross attention: Deep fusion transformer for image captioning. *IEEE Transactions on Circuits and Systems for Video Technology*, 2023.
- [Zhao *et al.*, 2021a] Hanqing Zhao, Wenbo Zhou, Dongdong Chen, Tianyi Wei, Weiming Zhang, and Nenghai Yu. Multi-attentional deepfake detection. In *IEEE Conference on Computer Vision and Pattern Recognition (CVPR)*, pages 2185–2194, 2021.
- [Zhao *et al.*, 2021b] Hanqing Zhao, Wenbo Zhou, Dongdong Chen, Tianyi Wei, Weiming Zhang, and Nenghai Yu. Multi-attentional deepfake detection. In *CVPR*, 2021.
- [Zhao *et al.*, 2021c] Tianchen Zhao, Xiang Xu, Mingze Xu, Hui Ding, Yuanjun Xiong, and Wei Xia. Learning self-consistency for deepfake detection. In *Proceedings of the IEEE/CVF international conference on computer vision*, pages 15023–15033, 2021.